

# Spherical harmonic decomposition applied to spatial-temporal analysis of human high-density EEG

Brett. M. Wingeier\*

*Brain Sciences Institute, Swinburne University of Technology,  
400 Burwood Road, Hawthorn, Victoria 3122, Australia.*

Paul. L. Nunez

*Department of Biomedical Engineering, Boggs Center, Tulane University,  
New Orleans, Louisiana, 70118.*

Richard. B. Silberstein

*Brain Sciences Institute, Swinburne University of Technology,  
400 Burwood Road, Hawthorn, Victoria 3122, Australia.*

(October 30, 2018)

## Abstract

We demonstrate an application of spherical harmonic decomposition to analysis of the human electroencephalogram (EEG). We implement two methods and discuss issues specific to analysis of hemispherical, irregularly sampled data. Performance of the methods and spatial sampling requirements are quantified using simulated data. The analysis is applied to experimental EEG data, confirming earlier reports of an approximate frequency-wavenumber relationship in some bands.

## I. INTRODUCTION

The human electroencephalogram (EEG), as measured at the scalp, represents a superposition of electric fields resulting from post-synaptic potentials in neocortex, the thin (2 to 5 mm) surface layer of human brains. Several models of neocortical dynamics treat EEG as a mixed global/local phenomenon [1–3], and a better understanding of its spatial-temporal dynamics is necessary for evaluation and refinement of these models. Its temporal behavior has been studied at length, both by clinical observation [4] and with such tools as power spectra [5], coherence [6], the Hilbert transform [7], and many others. However, until recently poor spatial resolution (due to minimal electrode sampling and under-use of head models) has limited spatial analysis of EEG [1,2,8].

As a potential field on a near-hemispherical surface, EEG is amenable to analysis by spherical harmonic decomposition. In this paper, we apply two methods of decomposition (one described by Cadusch [9] and one adapted from Misner [10]) to 131-channel EEG data. Using simulated data, we discuss issues and pitfalls relevant to such an analysis, specifically the effects of limited and irregular sampling density, integration over a hemisphere, and deviations from a spherical surface. From the experimental data, we then draw conclusions regarding the frequency-wavenumber relation of neocortical activity.

## II. METHOD

We use the real spherical harmonics [11], defined on the sphere  $\Omega$  and described by the orthogonality integral

$$\langle Y_{lm} | Y_{l'm'} \rangle = \int_0^{2\pi} \int_0^\pi Y_{lm}(\theta, \phi) Y_{l'm'}(\theta, \phi) \sin \theta d\theta d\phi = \delta_{l,l'} \delta_{m,m'}. \quad (1)$$

In theory, a potential field  $\Phi(\Omega)$  may be decomposed into spherical harmonic amplitudes  $\Phi_{lm}$  defined by

$$\Phi_{lm} = \int_{\Omega} Y_{lm}(\theta, \phi) \Phi(\theta, \phi) d^2\Omega. \quad (2)$$

In the example of EEG and similar data we encounter three major and two minor issues.

### A. Sampling

First, when attempting to decompose experimental data, we sample  $\Phi(\Omega)$  at specific locations  $\Gamma$ . Assuming near-regularly spaced electrodes, our maximum resolvable  $l$  is determined by a spherical analog of the familiar Nyquist limit [12]  $f_{max} = 1/(2\Delta T)$ . With mean angular inter-electrode distance  $\gamma$ , we initially adopt a conservative limit of

$$l_{max} = \left\lceil \frac{\pi}{2\gamma} \right\rceil, \quad (3)$$

or  $l_{max} = 6$  for our 131-channel electrode cap. Analog pre-filtering to avoid spatial aliasing is not required here due to the low-pass characteristics of the head volume conductor [13].

## B. Regularization

With sampled data  $F(\Gamma)$ , the discretized version of the decomposition in Eq. 2 is unstable in higher  $l$ -indices. (An apparently accurate reconstruction of the signal may be generated, with large artifacts in the higher spatial frequencies.) We must invoke constraint or regularization techniques to address this issue. Cadusch *et al* [9] approached the problem as a side issue of spherical spline interpolation. The estimate  $\hat{\Phi}_{lm}$  is constrained by the spline constraints, and the problem for a given sampling grid and  $l_{max}$  is reduced to a multiplication by a matrix of  $\mu_{lm}$  coefficients:

$$\hat{\Phi}_{lm} = \sum_{x \in \Gamma} \mu_{lm}(x) F(x). \quad (4)$$

Recently, Misner [10] introduced a more complex method for decomposition on a rectangular three-dimensional grid; that is, generalized to use  $Y_{nlm}(r, \theta, \phi)$ . We implement here the special case of sampling on a spherical surface, more relevant to EEG analysis, in which  $r$  is constant. In Misner's method, a correction matrix of  $G_{AB}$  accounts for discretization and limited sampling:

$$G_{AB} = \sum_{x \in \Gamma} Y_A(x) Y_B(x) w_x, \quad (5)$$

where A and B refer to index groups ( $lm$ ). Here we use the real harmonics and replace Misner's weight function  $w_x$  with the effective area of each electrode.  $G^{AB}$ , the matrix inverse of the  $G_{AB}$ , is used to calculate "adjoint spherical harmonics"  $Y^A$ . Finally, a set of coefficients  $R_{lm}$ , analogous to Cadusch'  $\mu_{lm}$ , is generated and used as in Eq. 4 to estimate  $\hat{\Phi}_{lm}$ .

## C. Hemispherical sampling

Particularly relevant to EEG analysis is the error introduced by sampling over only half of the sphere. This sampling corresponds to only  $\frac{1}{2}$  of a spatial cycle of the  $l = 1, m = 0$  function, suggesting potential accuracy problems for functions involving  $l = 0$  and 1. It is also clear that the functions  $Y_{lm}$  will no longer be orthonormal for  $0 \leq \theta \leq \pi/2$  only; rather, we replace the  $\delta$  in Eq. 1 with an error quantity  $\epsilon$ :

$$\langle Y_A | Y_B \rangle = \int_0^{2\pi} \int_0^{\frac{\pi}{2}} Y_A(\theta, \phi) Y_B(\theta, \phi) \sin \theta d\theta d\phi = \epsilon_{AB}. \quad (6)$$

In general, our hemispherical estimates  $\hat{\Phi}'_A$  will be related to the hypothetical full-sphere result by the matrix of  $\epsilon_{AB}$ 's:

$$\hat{\Phi}' = \epsilon \hat{\Phi} \quad (7)$$

and our  $\hat{\Phi}'_A$  become somewhat ambiguous between certain sets of  $(l, m)$ . Although it may seem appropriate to invert  $\epsilon$  and calculate a more accurate result, the matrix is ill-conditioned ( $R > 10^8$ , where the 2-norm condition number  $R$  is the ratio of the largest singular value of  $\epsilon$  to the smallest) and thus the inversion is problematic.

In addition, if we use the hemispherical region to calculate Misner’s  $G_{AB}$  in Eq. 5, the resulting matrix of  $G_{AB}$  is ill-conditioned ( $R > 10^8$ ) and thus the  $G^{AB}$  cannot be reliably found. Rather, we created a mirrored set of electrodes  $\Gamma'$ , calculated the matrix  $\mathbf{R}$  of  $R_{lm}$  for sample set  $(\Gamma \cup \Gamma')$ , and discarded the antipodal rows of  $\mathbf{R}$ . Cadusch’ spline method, while still subject to Eq. 7, is native to the hemispherical surface and requires no further manipulation.

#### D. Coordinate orientation

In many problems, the sphere has no preferred direction. The  $m$ -indices are usually collapsed [14] to produce an angular power spectrum estimate  $\hat{G}(l)$  as a function of wavenumber  $l$ :

$$\hat{G}(l) = \sum_{m=-l}^l (\hat{\Phi}'_{lm})^2 \quad (8)$$

which is independent of coordinate system orientation. As well, we found the “hemispherical error” in  $l$ -spectrum to be independent of orientation. In some EEG studies, of course, the orientation of the underlying cerebral hemispheres may be relevant. In such cases, local spatial Fourier analysis [1] should adequately complement our decomposition without the complication of distinguishing  $m$ -modes.

#### E. Non-spherical media

We assume that our medium  $\Omega$  is a sphere, whereas biological data is often sampled on an irregular surface. The upper surface of the “average” human head [15] may be represented as a hemiellipsoid with axes  $a = 10.52$  cm,  $b = 7.66$  cm, and  $c = 8.41$  cm, or alternatively 25%, -9%, and 0% elongation from a perfect sphere. Although prolate spheroidal harmonics have been applied to biophysical field problems [16–18], the technique is often unwieldy. In comparison to error from  $\epsilon_{AB}$ , especially for low  $l$ , we assume the error due to approximating the ellipsoidal surface with a spherical surface is negligible.

### III. APPLICATION TO SIMULATED DATA

We generated evenly tessellated, hemispherical electrode maps of 74, 187, 282, and 559 electrodes, in addition to common experimental maps of 20, 64, and 131 [8] electrodes. Five hundred potential maps were simulated for each electrode configuration. Each potential map was randomly generated with harmonics of degree  $l = 6$ , such that the  $\Phi_{lm}$  varied with uniform distribution between 0 and 1. Power spectrum estimates  $\hat{G}(l)$  were then calculated for each map, using both methods. Figure 1 shows Pearson’s correlation coefficients  $r_l$ , calculated between  $G(l)$  and  $\hat{G}(l)$  over the 500 trials for each electrode map.

We have noted that the error due to  $\epsilon_{AB}$  causes power from one  $(l, m)$ -component to be misinterpreted as power in another, often of different  $l$ . Therefore, we might expect either method’s performance to depend on the  $l$ -spectrum being analyzed. Using preliminary

experimental data, we constructed an approximate power spectrum  $G_{norm}(l)$  for average-referenced scalp EEG, peaked at  $l = 1$  and  $l = 2$ , and decaying with  $l^{-1}$  thereafter. Another five hundred potential maps were generated, with  $\Phi_{lm}$  uniformly distributed between

$$0 < \Phi_{lm} < \frac{G_{norm}(l)}{2l + 1} \quad (9)$$

to simulate a physiologically realistic distribution of  $l$ -spectra. Power spectrum estimates  $\hat{G}(l)$  were calculated for each map using both methods. Results are shown in Fig. 2.

In general, results for the spline method — though often quite accurate — were dependent on the distribution of  $l$ -spectra being measured, exact electrode positions, and electrode numbers. Results for the adjoint harmonic method seemed more robust, even for sparse ( $n = 64$ ) sampling, although accuracy was somewhat less in the higher harmonics.

In both methods, for  $l = 6$  we observed minimal improvement for more than 131 electrodes. We thus believe that our 131-channel sampling is an appropriate tool for further study. Furthermore, given the limit in Eq. 3 and the known volume-conductor attenuation of higher modes [13], we suggest that study of spatial frequencies higher than approximately  $l = 8$  will be better served by intracranial EEG than by denser electrode maps.

In general, for low  $l$  the adjoint harmonic method seemed more consistent. We examined typical 131-channel decompositions (Fig. 3) to investigate further. Both methods accurately reproduced the potential maps ( $r > 0.9$  for 131 channels). The spline method, however, was slightly unstable for low  $l$ , and the erroneous negative  $\hat{\Phi}_{lm}$  are reflected in the power spectrum.

#### IV. REFINEMENTS AND ANALYSIS OF ERROR

Any application of the spherical harmonic decomposition should take into account the estimated relative contribution of various error sources. Aside from measurement and experimental error, these may be divided into three categories: sampling error, orientation error, and hemispherical error.

##### A. Sampling error

Figures 1 and 2 indicate minimal improvement for  $l \leq 6$  with more than 131 electrodes. We can thus deduce that the Nyquist-like limit in Eq. 3 is an appropriate guideline. When using coarser sampling, we expect some decrease in performance for higher  $l$ . Decreased accuracy for 20, 64, and 74 channels (seen in Figs. 1 and 2, particularly for 20 channels) may be attributed to sampling error.

##### B. Orientation error

For a given  $l$ -spectrum, results will vary if power is randomly distributed across the  $m$ 's; that is, various  $m$ -components interact differently with our hemispherical sample grid. Five

hundred random  $l$ -spectra, with realistic distribution of  $G(l)$ , were generated. Thirty 131-channel maps, randomly varying in  $m$ -power, were generated for each original  $l$ -spectrum. Figure 4 displays the resulting accuracy, again shown as correlation coefficient  $r_l$  between  $G(l)$  and  $\hat{G}(l)$  over the 100 trials.

Very little is gained in this simulation by decomposition of multiple epochs. As described in the following section, error due to  $m$ -distribution of power is largely swamped by hemispherical error. In practice, however, we must emphasize (in the presence of random measurement noise) the importance of averaging decompositions across many epochs. Orientation error will also become significant if our sampling grid is severely non-uniform.

### C. Hemispherical error

In Sec. II above, we have discussed the hemispherical error  $\epsilon_{AB}$ . Although it is impossible to improve our decomposition results by inverting the matrix  $\epsilon$ , we may generate a corresponding matrix for the power spectrum result and use it to estimate the contribution of hemispherical error.

Power in a single harmonic  $Y_{lm}(\theta, \phi)$  is blurred by the hemispherical decomposition into surrounding harmonics. Using the 131-channel sampling map, we generated five hundred potential maps for each of  $l = 0 \dots 6$ , each with one unit power distributed randomly among the available  $m$ 's. By averaging over the five hundred resulting power spectra, for each  $l$ , we obtained an empirical ‘‘averaged blurring matrix’’  $\mathbf{E}$  for power spectra obtained from hemispherical decomposition. That is,

$$\hat{G}(l) \approx \mathbf{E}G(l). \quad (10)$$

The typical  $\mathbf{E}$  for both methods is a blurred identity matrix; that is, error in power spectra is largely between adjacent  $l$ . It is again tempting to invert  $\mathbf{E}$ , de-blur our spectra, and calculate a more accurate result, but although most  $\mathbf{E}$  are invertable we found that for realistic spectra the benefit was marginal at best. Instead,  $\mathbf{E}$  may be used to better understand the implications of hemispherical error.

We calculated correlation coefficients as in Fig. 4, between  $\mathbf{E}G(l)$  and  $\hat{G}(l)$  over the 500 trials of 30 epochs for 131 electrodes. The resulting higher correlations (although not applicable to a decomposition of real data) are plotted in Fig. 5. By comparison with Figs. 2a and 4, the result indicates the importance of hemispherical error. In particular, after examination of typical  $\mathbf{E}$  and  $\epsilon$  matrices, we may interpret the decreased performance at low  $l$  as blurring between adjacent wavenumbers. Furthermore, the increased effect, seen in Fig. 5, of averaging across various  $m$ -distributions indicates that some abrupt changes in performance may be attributed to sensitive interactions between  $\mathbf{E}$ -blurring and random  $m$ -distribution.

Practically, the near-identity character of  $\mathbf{E}$  is extremely useful. Hemispherical error manifests as blurring between adjacent  $l$ . Thus, we may expect composite measures such as the sum of power in  $l=0,1$  to be substantially more accurate than individual estimates. Figure 6 displays the accuracy of  $l=0,1$  and  $l=2 \dots 6$  adjoint harmonic power estimates (used below in our experimental trials), for 500 epochs, realistic  $l$ -distribution, and various sampling densities.

## V. APPLICATION TO EXPERIMENTAL DATA

Nunez in 1974 [19,20] and Shaw in 1991 [21], using Fourier analysis along linear electrode EEG arrays, observed a relationship between increasing spatial and increasing temporal frequency in the 8-13 Hz band, roughly consistent with simple wave dispersion relations. We attempted to duplicate this result in order to test the adjoint harmonic method under experimental conditions. We analyzed 131-channel EEG (resting, eyes closed) in five human subjects. Temporal Fourier coefficients were determined for 300 to 600 one-second epochs (depending on available data), and  $l$ -spectra averaged over these epochs.

Results are summarized in Fig. 7 as the ratio of power in low ( $l = 0, 1$ ) to power in high ( $l = 2, 3, 4, 5, 6$ ) spatial frequencies. Above approximately  $f = 8$  Hz, with increasing  $f$  we observed a general trend towards power in higher  $l$ . We also observed high-wavenumber power in the delta band ( $f \leq 3$  Hz). The alpha band (c. 8–13 Hz) was characterized by the highest power in low spatial frequencies.

In order to rule out methodological artifact, we generated and analyzed 300 seconds of simulated EEG using 3602 uncorrelated sources, each generating  $1/f$  noise through a head volume conductor model as described in [13]. As expected, the EEG-like noise (labeled RND in the figure) showed no relation between spatial and temporal frequencies.

## VI. CONFIDENCE INTERVAL ESTIMATION

Estimates of the temporal power spectrum are known to vary in chi-square distribution [12], assuming normally distributed estimates of the underlying Fourier coefficients. Error distribution for spatial spectrum estimates, on the other hand, is complicated by the dependence of hemispherical and orientation error on the entire  $l$ -spectrum. For composite measures of both spatial and temporal spectra, such as shown in Fig. 7, the situation becomes even more problematic. We propose an empirical test for estimation of such confidence levels, analogous to the randomization tests commonly applied in nonparametric statistical analysis [22].

Let

$$A = \frac{G_{01}}{G_{2...6}}, \quad (11)$$

where  $G_{01}$  is the total power in harmonics  $l=0$  and  $l=1$ , and  $G_{2...6}$  is the total power in harmonics  $l=2$  through  $l=6$ . Let  $\hat{G}_{01}$ ,  $\hat{G}_{2...6}$ , and  $\hat{A}$  represent estimates of the same. Above, we calculated  $\hat{A}_f$  for various temporal frequencies. Here, we calculate an approximate 95% confidence interval for single-epoch estimates of the actual  $A_f$ . The confidence interval will apply only to the spatial spectrum composite measure, neglecting error (or nonstationarity) in temporal frequency spectra, which for many applications may be as important. Note, though, that for 300 epochs the normalized standard error of a temporal power spectrum estimate is less than 6%.

To determine an empirical confidence interval, we would typically examine the distribution of random re-samples. In this application, we created many random  $l$ -spectra from an estimated distribution of  $l$ -power, simulated many decompositions, and examined the resulting distribution as follows.

Since hemispherical error is dependent on  $l$ -spectrum, the result will be influenced by the distribution of the random spectra. Srinivasan *et al* [13] analytically estimated the spatial frequency domain transfer function for volume-conduction blurring of scalp potential as proportional to  $(2l+1)^{-1}$ . This “spatial smearing” is due mainly to the poorly conducting skull and physical separation between cortical current sources and scalp electrodes. In our calculation, we assumed that underlying  $l$ -spectra vary in uniform distribution in proportion to  $(2l+1)^{-1}$ , and that with average-referenced data the contribution of  $l=0$  is negligible. A large number (20,000) of  $l$ -spectra were generated, randomly selecting for each  $l$ -bin a value from the appropriate distribution. The decomposition was performed, and the composite measure  $A$  calculated, for each randomized spectrum.

By examining the distribution of known surrogate  $A_{rand}$  which produce a certain estimate  $\hat{A}_{rand}$ , we can estimate an empirical confidence interval for our spectral estimate. In Fig. 8, we show the scatter plot of  $A_{rand}$  against  $\hat{A}_{rand}$  with 95% confidence intervals. For a given estimate  $\hat{A}$  and the assumptions discussed above, 95% of the time, the actual  $A$  will fall between the two lines shown.

A similar procedure may be used to calculate confidence intervals for other measures, whether the actual  $G_l$  or other composite measures. Careful judgment must be applied when estimating confidence intervals for multiple-epoch measures such as shown in Fig. 6. As demonstrated earlier in this paper, variation in the  $m$ -component of an  $l, m$ -spectrum only allows us to “average out” the minimal orientation error. Variation in hemispherical error (dependent on  $l$ -spectrum), without gross violation of the stationarity assumption, is necessary for the average of estimates  $\hat{A}$  over multiple epochs to converge to  $A$ .

## VII. DISCUSSION

Our simulations provide a firm basis for application of spherical harmonic decomposition to irregularly sampled, hemispherical data such as EEG. Our hemispherical modification of Misner’s adjoint harmonic method [10] proved most consistent. However, for physiological data of known power distribution, the spline method [9] is complementary and may be slightly more accurate with high-density sampling. It seems that, within the conservative band-limit of equation [3] and the known spatial filter properties of the head [13], decomposition accuracy will not be materially improved by more than 131 electrodes for scalp EEG. We suggest that confidence intervals for such decompositions, or for decomposition-derived measures, be determined empirically using randomized data. Furthermore, while single-decomposition errors are relatively large, with multiple epochs the experimental accuracy may be increased substantially. For this averaging to be both valid and effective, we must assume a quasi-stationary wavenumber spectrum across our epochs, but with sufficient random variation in hemispherical error for our estimates to converge upon the mean. In addition, especially in EEG applications, we must remain aware of the limitations inherent in collapse across  $m$ ’s (we assume the orientation of the underlying cerebral hemispheres is irrelevant) and the use of spherical harmonics on a hemispheroidal surface.

The dynamical properties of human EEG rhythms are quite complicated, varying substantially between individuals and brain states. Furthermore, physiologically-based theoretical models point to substantial nonlinear effects and interactions across spatial scales



[2,23–26]. Despite all the obvious complications, results from the spherical harmonic decomposition of experimental EEG agreed qualitatively with crude linear electrode array results [1,21]. These results were seen in all subjects and are consistent with a mixed global/local model of cortical dynamics, in which lower global mode oscillations produce alpha rhythm, superimposed on local (spatially uncorrelated) activity in various frequency bands [2]. Further study of spatiotemporal EEG dynamics, using spherical harmonic decomposition, should shed more light on these issues.

#### **ACKNOWLEDGMENTS**

This work was supported by the Australian Research Council grant #A10019013 and by the U.S. National Science Foundation (B.M.W.).

## REFERENCES

- \* Also at Department of Biomedical Engineering, Tulane University; e-mail wingeier@bsi.swin.edu.au.
- [1] P. L. Nunez, *Electric Fields of the Brain: The Neurophysics of EEG* (Oxford University Press, New York, 1981).
  - [2] P. L. Nunez, *Neocortical Dynamics and Human EEG Rhythms* (Oxford University Press, New York, 1995).
  - [3] F. H. Lopes da Silva, in *Neocortical Dynamics and Human EEG Rhythms*, by P. L. Nunez (Oxford University Press, New York, 1995).
  - [4] K. E. Misulis, *Essentials of Clinical Neurophysiology* (Butterworth-Heinemann, Boston, 1997).
  - [5] W. Klimesch, *Brain. Res. Rev.* **29**, 169 (1999).
  - [6] P. L. Nunez *et al.*, *Electroen. Clin. Neuro.* **103**, 516 (1997).
  - [7] Tass P *et al.*, *Phys. Rev. Lett.* **81**, 3291 (1998).
  - [8] P. L. Nunez, B. M. Wingeier, and R. B. Silberstein (unpublished).
  - [9] P. J. Cadusch, W. Breckon, and R. B. Silberstein, *Brain Topogr.* **5**, 59 (1992).
  - [10] C. W. Misner, <http://xxx.lanl.gov/abs/gr-qc/9910044>, 1999.
  - [11] M. Boas, *Mathematical Methods in the Physical Sciences* (J. Wiley & Sons, New York, 1983), p. 568.
  - [12] J. S. Bendat and A. G. Piersol, *Random Data* (J. Wiley & Sons, New York, 1986).
  - [13] R. Srinivasan, P. L. Nunez, D. M. Tucker, R. B. Silberstein, and P. J. Cadusch, *Brain Topogr.* **8**, 355 (1996).
  - [14] P. J. E. Peebles, *Astrophys. J.* **185**, 413 (1973).
  - [15] S. K. Law and P. L. Nunez, *Brain Topogr.* **3**, 365 (1991).
  - [16] G. C. K. Yeh and J. Martinek, *Ann. NY. Acad. Sci.* **67**, 1003 (1957).
  - [17] B. N. Cuffin and D. Cohen, *IEEE Trans. Biomed. Eng.* **24**, 372 (1977).
  - [18] J. C. de Munck, *J. Appl. Phys.* **64**, 464 (1988).
  - [19] P. L. Nunez, *Math. Biosci.* **21**, 279 (1974).
  - [20] P. L. Nunez, *IEEE Trans. Biomed. Eng.* **21**, 473 (1974).
  - [21] G. R. Shaw, Ph.D. thesis, University of Alberta, 1991.
  - [22] E. S. Edgington, *Randomization Tests* (Marcel Dekker, New York, 1987).
  - [23] V. K. Jirsa and H. Haken, *Physica D* **99**, 503 (1997).
  - [24] V. K. Jirsa, R. Friedrich, H. Haken, and J. A. S. Kelso, *Biol. Cybern.* **71**, 27 (1995).
  - [25] L. Ingber, *Physica D* **5**, 83 (1982).
  - [26] L. Ingber, in *Neocortical Dynamics and Human EEG Rhythms*, by P. L. Nunez (Oxford University Press, New York, 1995).

## FIGURES

FIG. 1. Correlations between actual and estimated  $l$ -power for uniformly distributed random spectra. Five hundred potential maps were generated from known wavenumber spectra, with random power in each  $l$ -component, uniformly distributed between 0 and 1. For each of seven electrode densities, wavenumber spectra were estimated by spherical harmonic decomposition of the 500 sampled maps. Correlations between actual power and estimated power were calculated over the 500 trials for each  $l$ -component. Shown here for (a) adjoint harmonic and (b) spline methods, these correlations are a measure of the quality of a single decomposed power spectrum.

FIG. 2. Correlations between actual and estimated  $l$ -power for more realistically distributed random spectra based on genuine EEG data. As in Fig. 1, but in original spectra random power in each  $l$ -component is uniformly distributed between 0 and  $(2l + 1)^{-1}$ .

FIG. 3. Topography (left column),  $l, m$ -spectra (center column), and  $l$ -power (right column) for a typical 131-channel spherical harmonic decomposition. The original map is shown in (a). The adjoint harmonic method (b) reconstructs topography and gives an approximation of  $l$ -spectrum. Although the spline method (c) also reconstructs potential topography, we observe irregularities in the lower  $l$  amplitude estimates that contribute to decreased performance for these wavenumbers, and a less accurate  $l$ -spectrum estimate.

FIG. 4. Correlations between actual and estimated  $l$ -power for multiple-epoch, adjoint-harmonic estimates of the same  $l$ -spectrum, with epochs varying only in  $m$ -component. For a reasonably isotropic and dense sample array, such as the 131-channel EEG grid used here, there is little orientation error and thus little improvement in results.

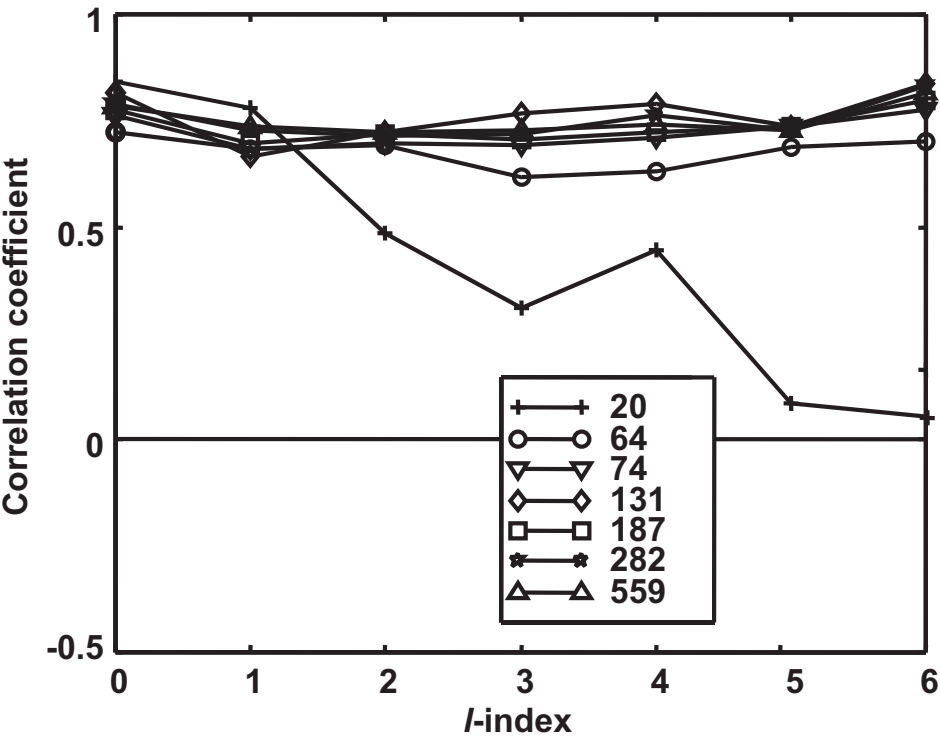
FIG. 5. Sampling a full sphere with 262 channels and the adjoint harmonic method, correlations between actual and estimated  $l$ -power are shown for multiple-epoch (varying only in  $m$ -component) estimates of the same  $l$ -spectrum. By sampling over the full sphere, we eliminate hemispherical errors illustrated in Fig. 4. Remaining errors are due to orientation (note improvement with multiple epochs) and imperfect sampling.

FIG. 6. Correlation coefficients, using the adjoint harmonic method, obtained by comparisons of estimated to actual summed power measures. The solid line represents power in  $l=0$  and  $l=1$  modes, and the broken line represents power summed over modes  $l=2$  through  $l=6$ . Increased accuracy (as compared to part A of Fig. 2) is because most hemispherical error manifests as blurring between power in adjacent  $l$ 's.

FIG. 7. Five to ten minutes of resting, eyes-closed EEG were collected with 131 channels from each of six subjects (one duplicated). Complex temporal Fourier coefficients were calculated for one-second epochs and subjected to spherical harmonic spatial decomposition using the adjoint harmonic method. Resulting wavenumber spectra were averaged for each 1-Hz band over the 300 to 600 epochs. The ratio of power in  $l=0,1$  to  $l=2,3,4,5,6$  is plotted as a simple indicator of a bias toward higher spatial frequencies at higher temporal frequencies (greater than about 10 Hz). This result is qualitatively consistent with the postulated existence of an approximate EEG dispersion relation, perhaps with alpha rhythm (8–13 Hz) representing the fundamental and lower overtones. A surrogate signal (dotted line), composed of random EEG-like noise and subjected to the same analysis, showed no such relation.

FIG. 8. 95% confidence intervals for single-epoch estimates of the power ratio  $A = G_{l=0,1}/G_{l=2..6}$ . Twenty thousand potential maps were generated from known, random, realistically distributed (based on genuine EEG data)  $l$ -spectra, and decomposed using 131 channels and the adjoint harmonic method. Here, known  $A$  are plotted against the resulting estimated  $A$ . Solid lines indicate the empirical 95% confidence interval for a given estimate of  $A$ . Multiple-epoch estimates will result in much smaller intervals, depending on the variation in  $l$ -spectra being decomposed.

**(a)** Adjoint harmonic method, uniform  $l$ , correlation between actual and estimated power



**(b)** Spline method, uniform  $l$ , correlation between actual and estimated power

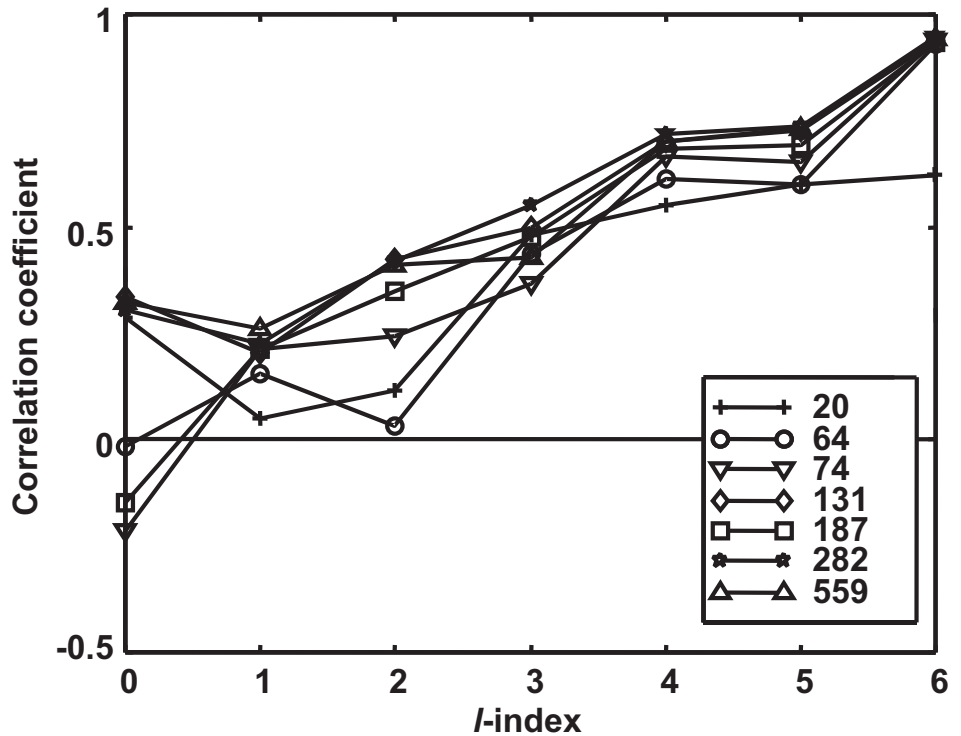
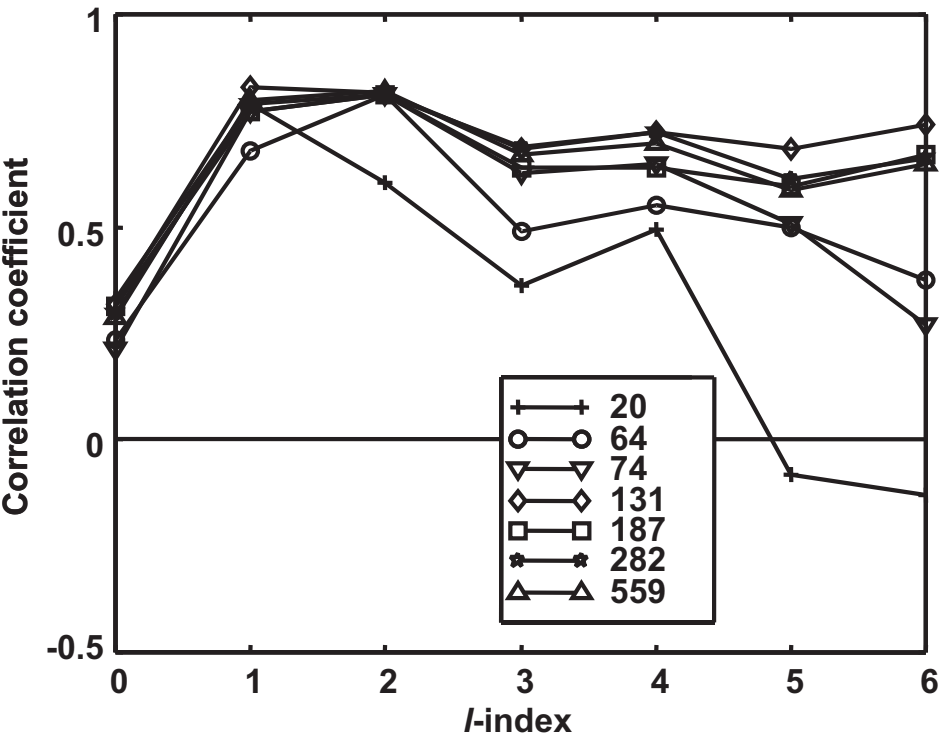


Figure 1 - Wingeier

two-column repro requested

**(a)** Adjoint harmonic method, realistic  $l$ , correlation between actual and estimated power



**(b)** Spline method, realistic  $l$ , correlation between actual and estimated power

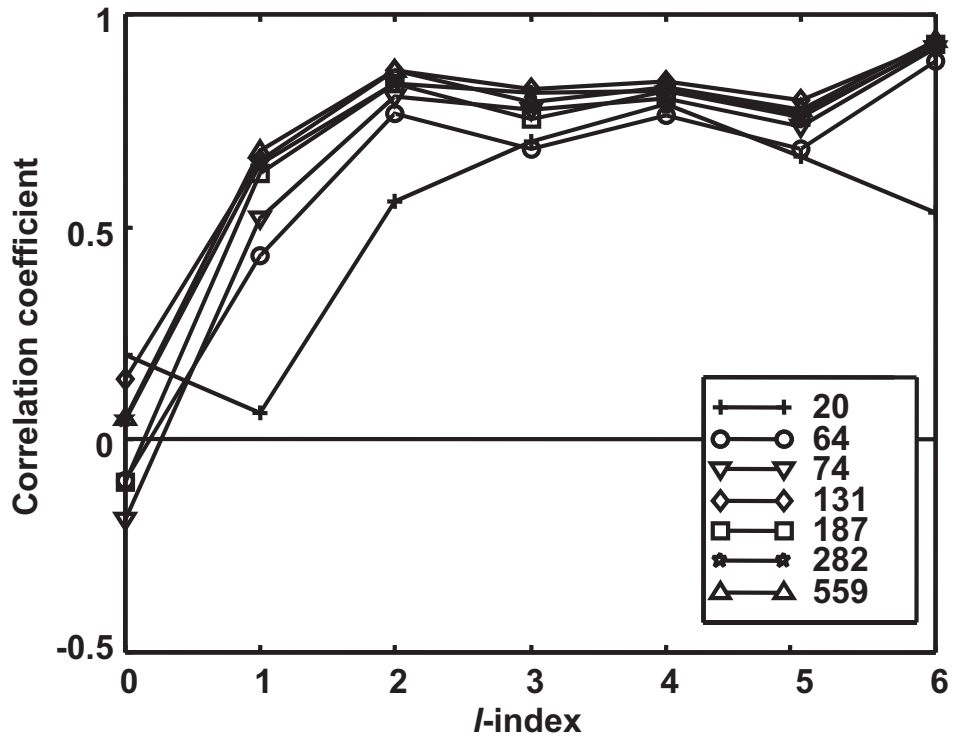


Figure 2 - Wingeier

two-column repro requested

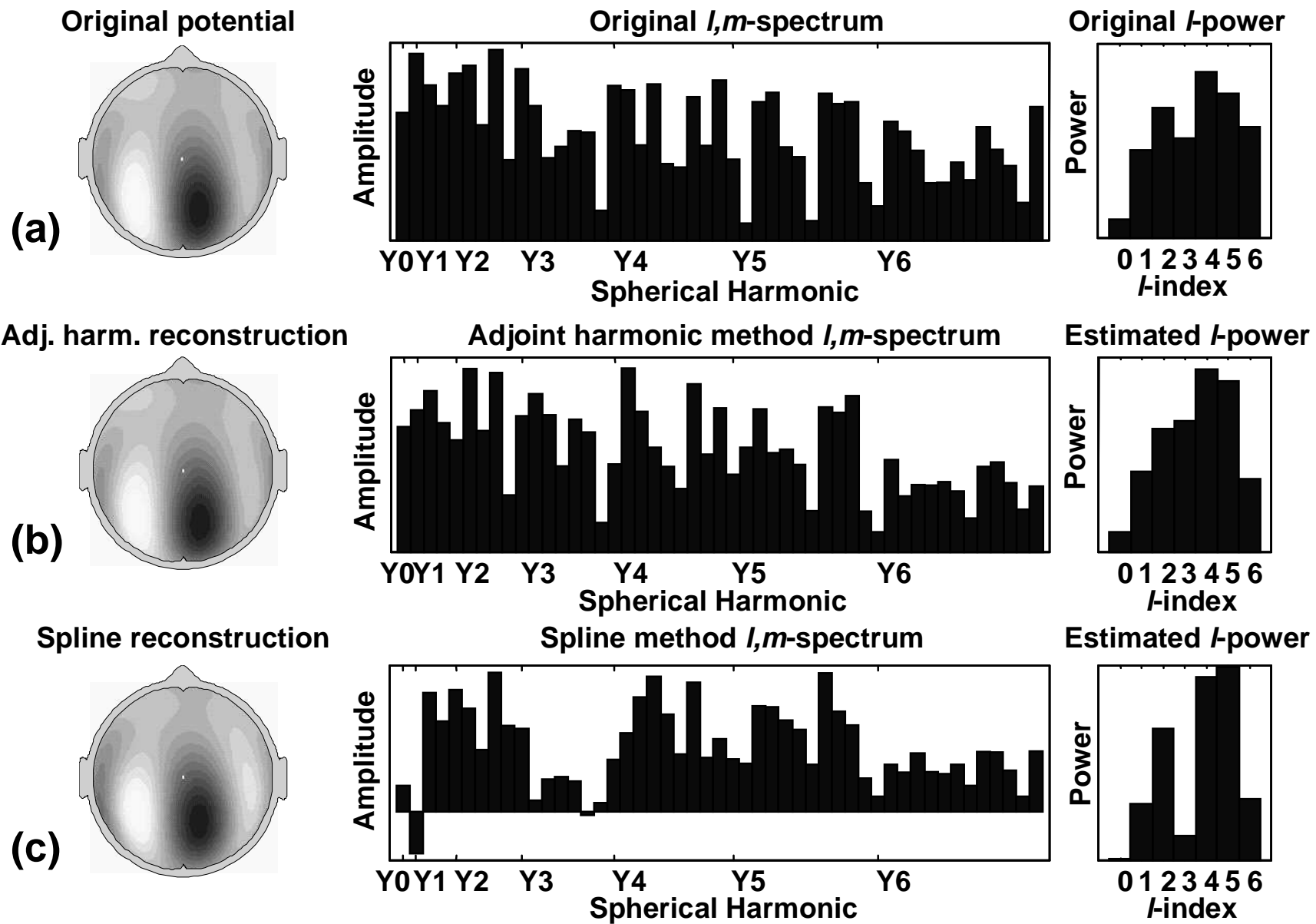


Figure 3 - Wingeier

two-column repro requested

Adjoint harmonic method, multiple epochs,  
correlation between actual and estimated power

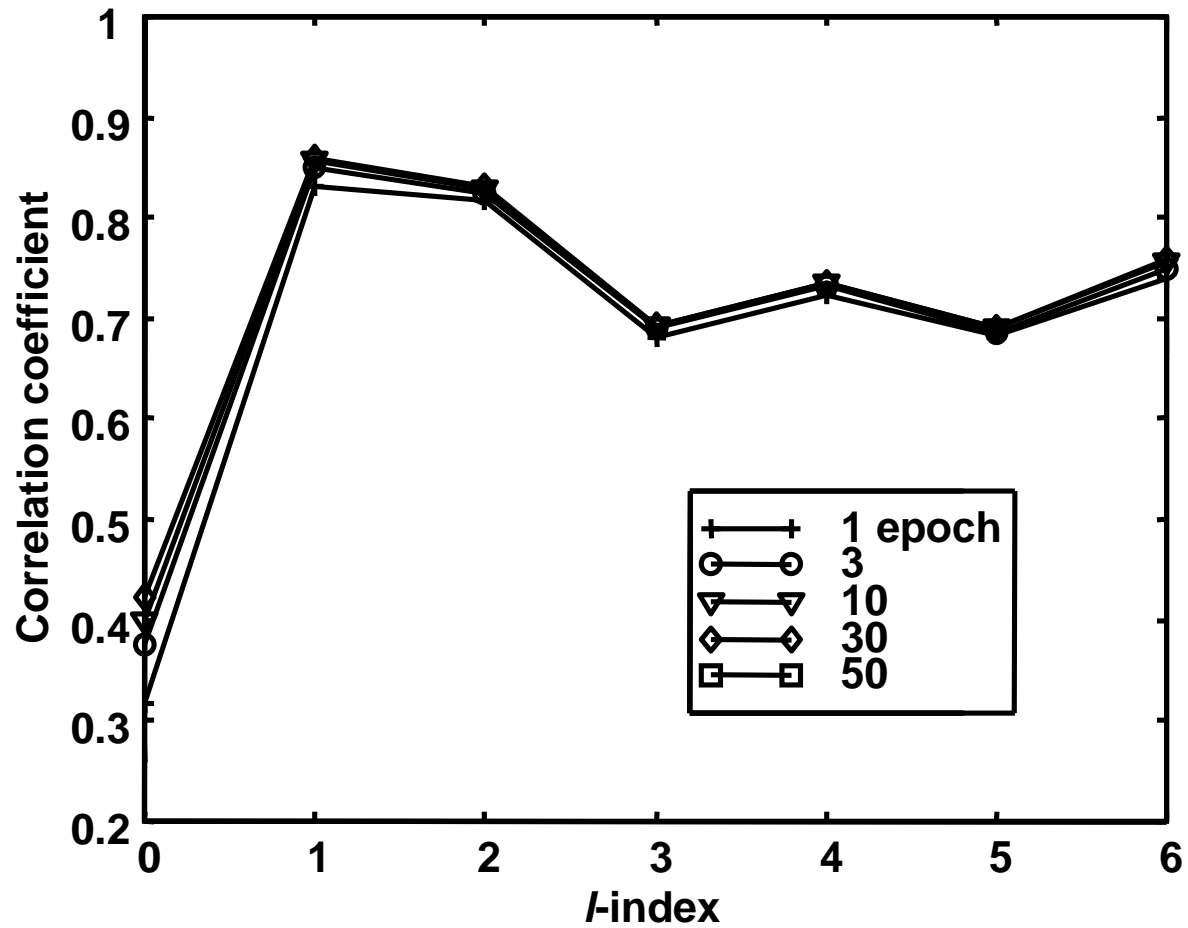


Figure 4 - Wingeier



Adjoint harmonic method, multiple epochs,  
simulation of no hemispherical error

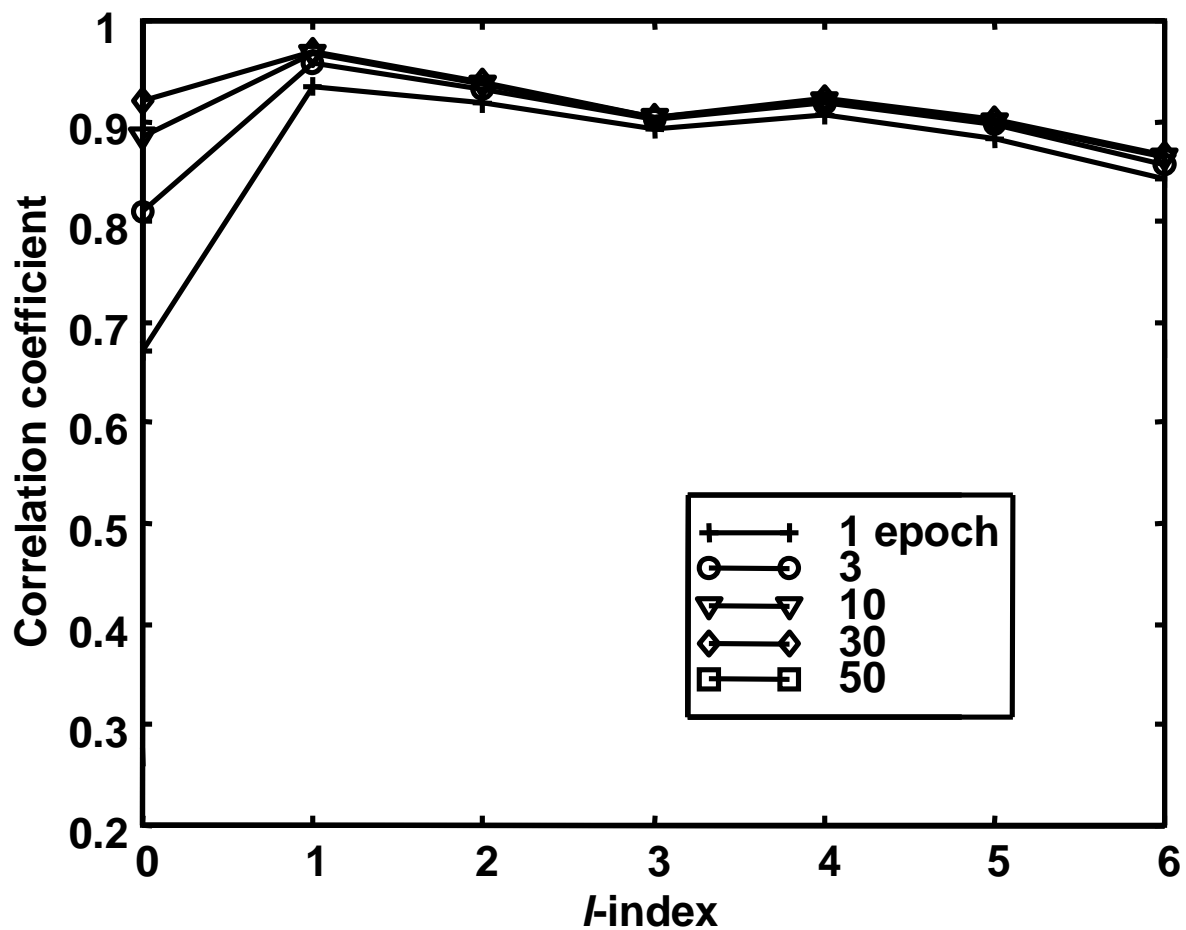


Figure 5 - Wingeier

Adjoint harmonic method,  
accuracy of composite measures

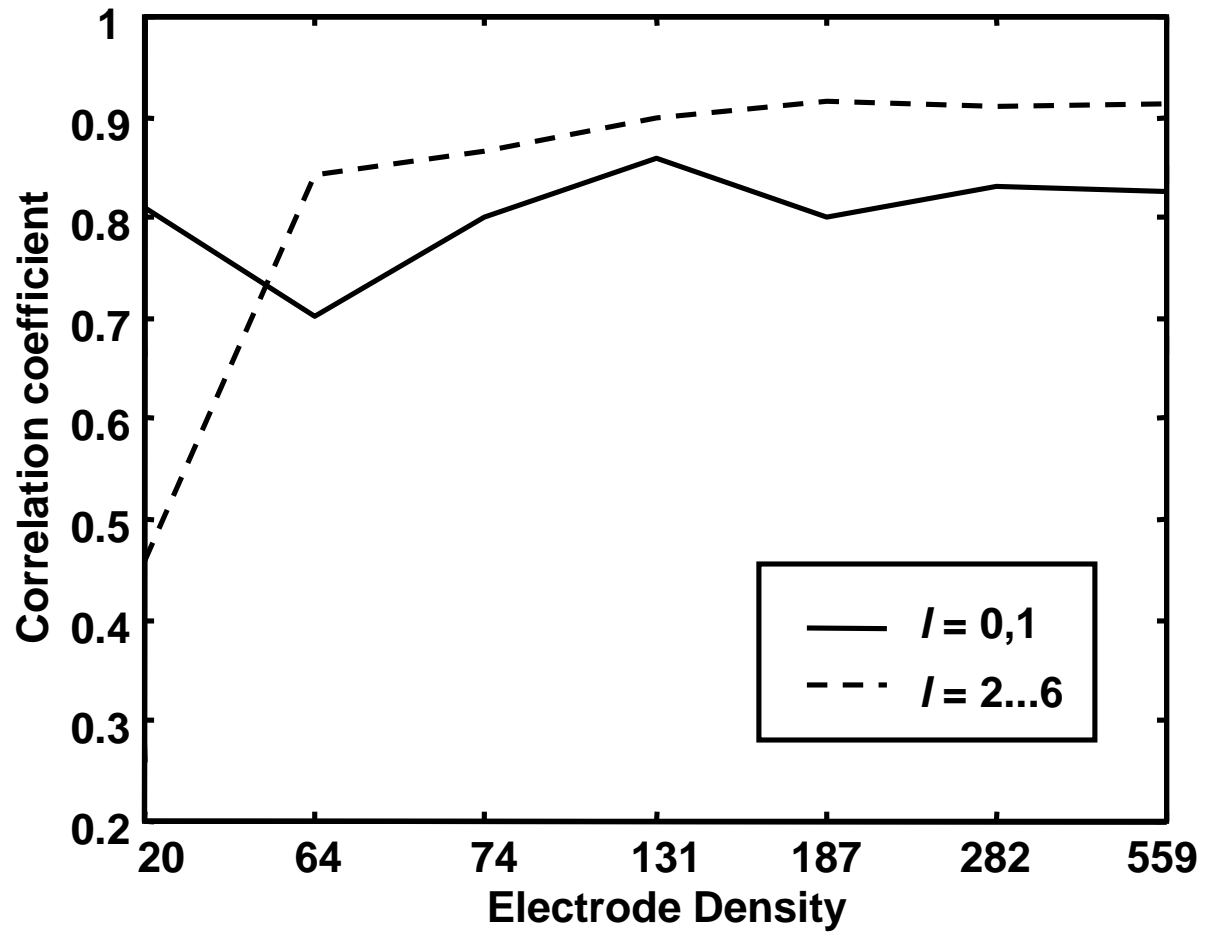


Figure 6 - Wingeier

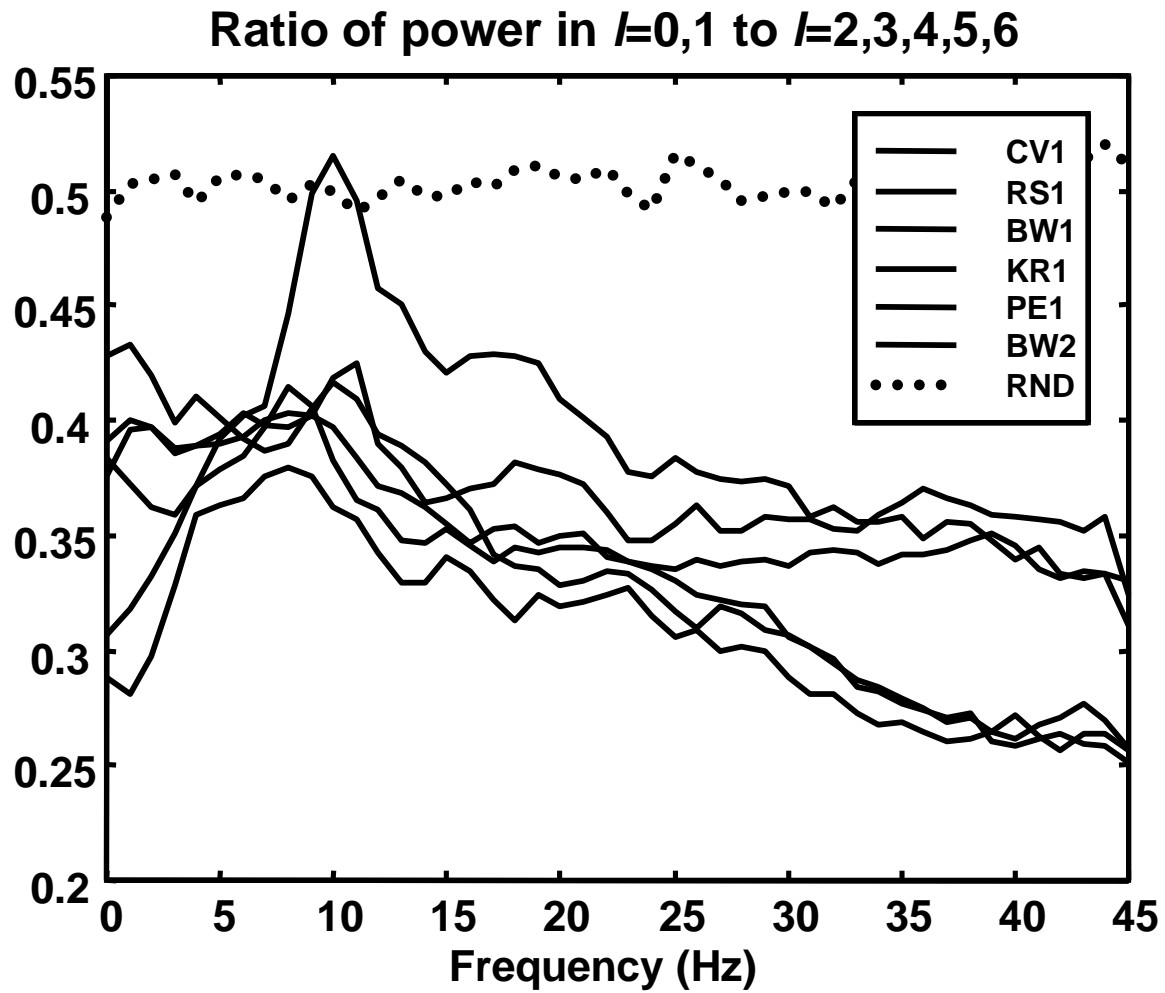


Figure 7 - Wingeier

Known v. estimated A - scatterplot  
and empirical 95% confidence interval

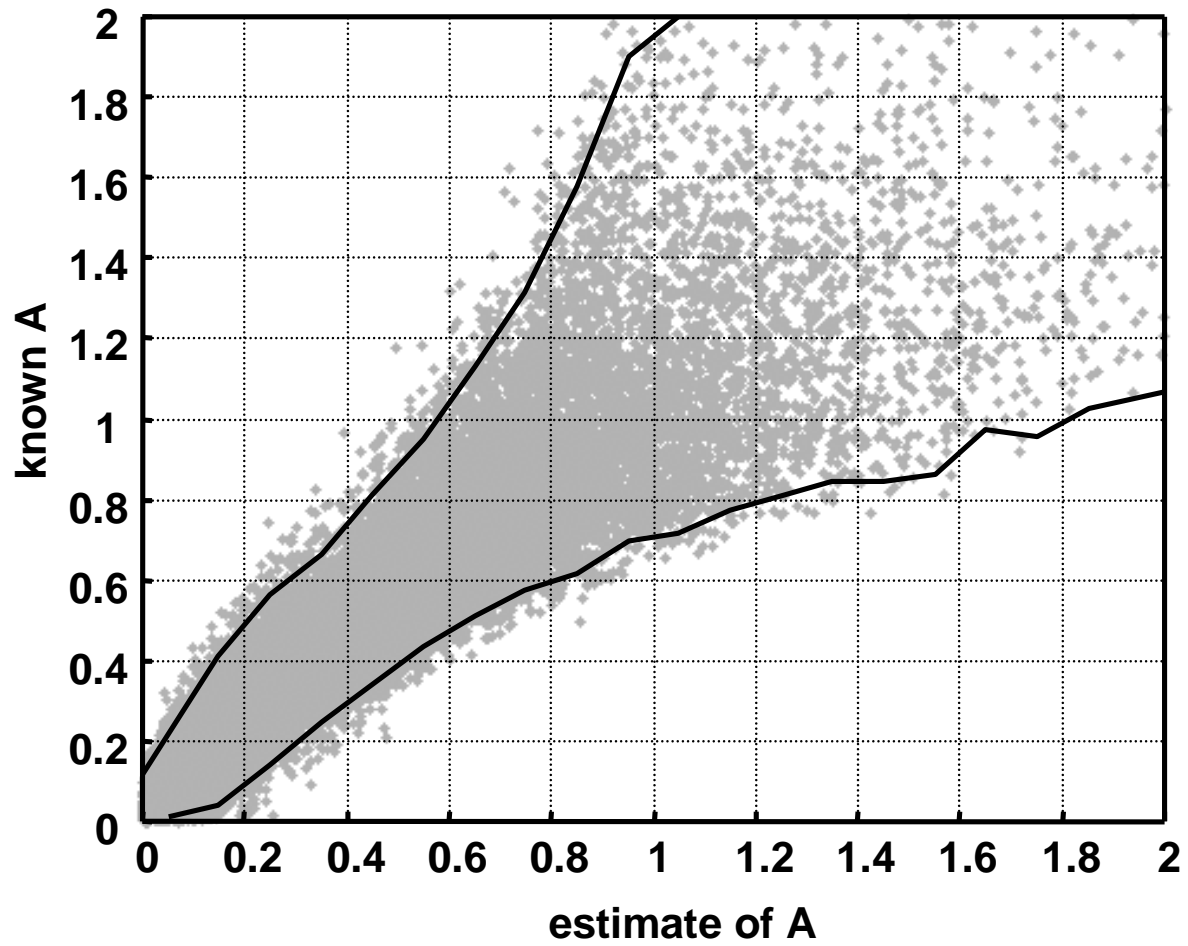


Figure 8 - Wingeier